Vesta's Pinaria Region: Original basaltic achondrite material derived from mixing upper and lower crust

L. A. McFadden[1], Jean-Philippe Combe[2], Eleonora Ammannito[3], Alessandro Frigeri[4], Katrin Stephan[5], Andrea Longobardo[4], Ernesto Palomba[4], Federico Tosi[4], Francesca Zambon[4], Katrin Krohn[5], Cristina M. DeSanctis[4], Vishnu Reddy[8], Lucille LeCorre[8], Andreas Nathues[6], Carle M. Pieters[7], Thomas Prettyman[8], C.A. Raymond[9], C.T. Russell[3]

1 NASA Goddard Space Flight Center, Greenbelt, MD 20771
2 Bearfight Institute, Winthrop, WA
3 IGPP, UCLA
4 INAF, Rome
5 DLR - German Aerospace Center, Institute of Planetary Research, Berlin, Germany
6 Max-Planck Institute for Solar System Research, 37077 Göttingen, Germany
7 Brown University, Providence RI
8 Planetary Science Institute, Tucson, AZ
9 Jet Propulsion Laboratory, California Institute of Technology, Pasadena, CA 91109

Corresponding Author:
Lucy A. McFadden
lucy.mcfadden@nasa.gov
Planetary Systems Laboratory, Code 693
Goddard Space Flight Center
8800 Greenbelt Rd
Greenbelt, MD 20771
301-614-6941

Abstract
Analysis of data from the Dawn mission shows that the Pinaria region of Vesta spanning a portion of the rim of the Rheasilvia basin is bright and anhydrous. Reflectance spectra, absorption band centers, and their variations, cover the range of pyroxenes from diogenite-rich to howardite and eucrite compositions, with no evidence of olivine in this region. By examining band centers and depths of the floor, walls and rims of six major craters in the region, we find a lane of diogenite-rich material next to howardite-eucrite material that does not follow the local topography. The source of this material is not clear and is probably ejecta from post-Rheasilvia impacts. Material of a howardite-eucrite

composition originating from beyond the Rheasilvia basin is evident on the western edge of the region. Overall, the Pinaria region exposes the complete range of basaltic achondrite parent body material, with little evidence of contamination of non-basaltic achondrite material. With both high reflectance and low abundance of hydrated material, this region of Vesta may be considered the "Pinaria desert".

1. Introduction

1.1. Background

Asteroid 4 Vesta had been identified as a basaltic achondrite parent body by McCord et al. (1970). Subsequent studies with ground-based telescopes (Gaffey et al. 1997) and Hubble Space Telescope (Binzel et al. 1997, Li et al. 2010) indicated that Vesta's southern hemisphere consisted of lower crustal and perhaps mantle material containing olivine. Basaltic achondrites consist of three meteorite types containing predominantly pyroxenes and plagioclase of different composition and relative abundances; they are known as HEDs (Duke and Silver, 1967, Consolmagno and Drake, 1977). The Dawn spacecraft orbited Vesta for 14 months from July 2011 to September 2012 with instruments designed to map its surface, including a visible and infrared spectrometer (VIR) for mineralogical studies, a framing camera (FC) with seven color filters for geomorphology and geological mapping, and a gamma ray and neutron detector (GRaND) to map elemental abundances (e.g. Prettyman et al. 2012, 2013). In addition, radiometric Doppler and range data and optical landmark tracking result in gravity maps (Konopliv et al. 2014) constraining the size of Vesta's metallic core, assuming the density of iron meteorites, to ~110 km (Raymond et al. 2014). Combining shape with gravity field and using densities derived from Howardite-Eucrite-Diogenite (HED) meteorites, further modeling suggests a thick crustal belt around two large impact basins (Ermakov et al. 2014, Raymond et al., 2014) named Rheasilvia and Veneneia. The thinnest crust is in the floor of these basins, and the data show that the core-mantle boundary remains below the surface supporting a three-layer model derived from petrology (e.g. Takeda, 1979) and consistent with the absence of olivine in the basin of these large craters (Ammannito et al. 2013).

In this paper, we explore the mineralogical composition of the Pinaria quadrangle of Vesta (Fig. 1; Roatsch et al. 2012) located between 0°-90° E longitude and 21°-66° S latitude in the Claudia coordinate system (Reddy et al. 2013; Russell et al. 2012). This region was previously only partially explored by Li et al. (2010) from Hubble Space Telescope color maps extending to 50° S (in the Thomas et al. 1997 coordinate system). In this paper we seek an understanding of the history and evolution of the asteroid that is known to be the basaltic achondrite parent body by addressing the following questions, offered as working hypotheses, arising from observing morphology (Fig. 1; Roatsch et al. 2012), topography (Fig. 2; Preusker et al. 2014), geology (Fig. 3; Krohn et al. 2014) and visible colors (Fig. 4; this work) in the Pinaria quadrangle. Spectroscopic data will allow us to test these hypotheses:

1. Do the six largest craters expose materials of different mineralogical compositions? Is there spectroscopic evidence that different compositional layers are probed by these impacts?

2. What is the nature of the mineralogical variation across the geological terrains, namely Rheasilvia ridge-and-groove terrain, the scarp wall material and the smooth plains beyond the Rheasilvia basin?

3. What do the answers to these questions tell us about this region, in comparison with the rest of Vesta?

To answer these questions, we examine radiometrically (Frigeri et al. 2015) and photometically (Li et al. 2013, Longobardo et al. 2014) corrected spectra extracted from VIR image cubes, spectral parameter maps displaying band 1 and band 2 centers and depths (Frigeri et al. 2015), and reflectance and 2.8 μm band depths (Combe et al. 2015, this issue). Spectral band parameters are related to mineralogical variations on Vesta's surface.
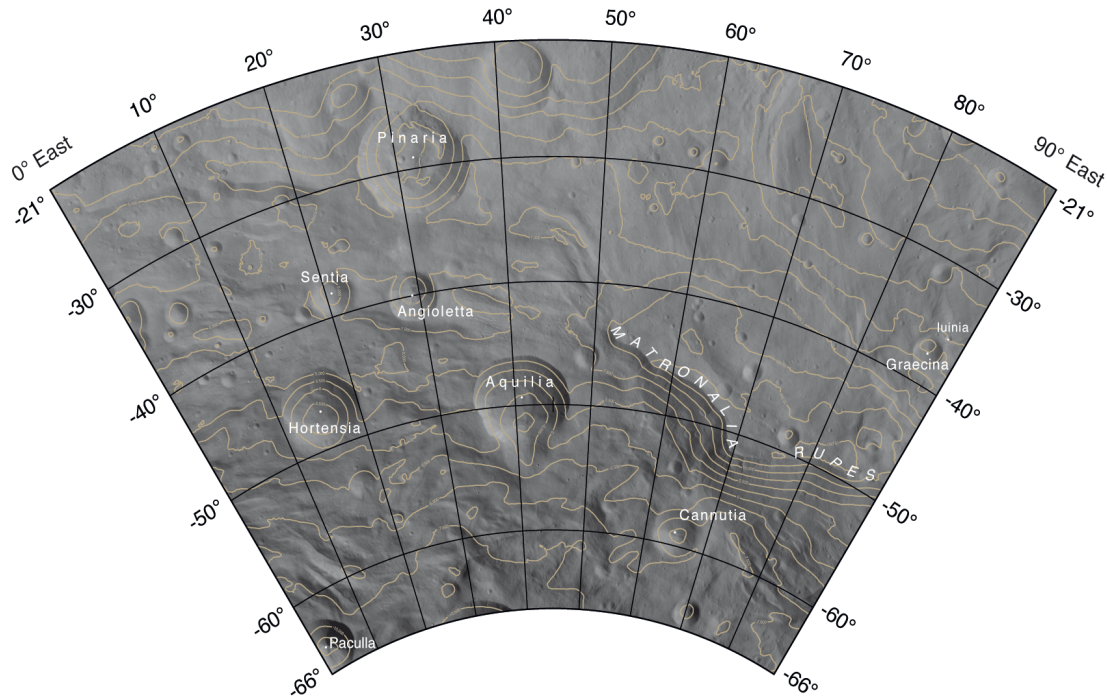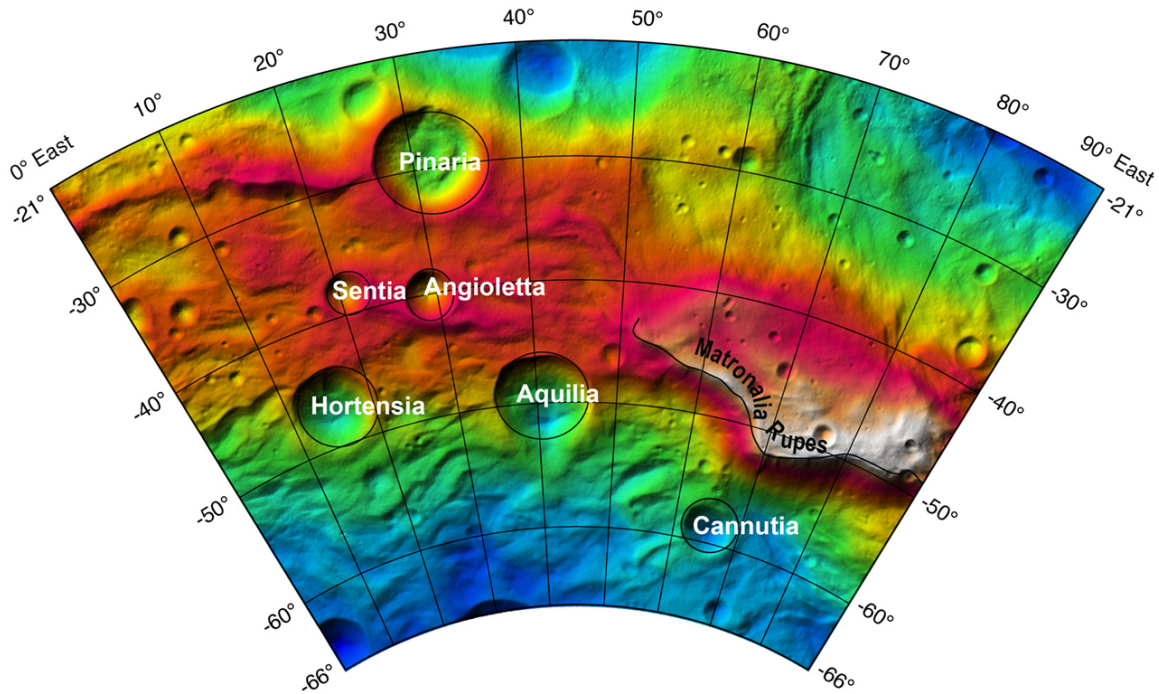

Fig. 1 Pinaria quadrangle map projection derived from ortho-rectified, clear filter images acquired during Dawn's high altitude mapping orbit. Map scale 1: 500,000 see Roatsch et al. 2012.

[Fig. 2 Shaded relief map of Pinaria quadrangle relative to Vesta's mean ellipsoid from Presuker et al. 2012]

1.2. Morphological and geological description

Within the Pinaria quadrangle is Matronalia Rupes (Fig. 3), which is the partial outer rim of the ~505 km south polar basin, named Rheasilvia (Schenk et al. 2012). It is elevated 16 km above the mean geoid of radii of 285 and 229 km and is the highest elevation on Vesta (Fig. 2). Spectral parameters of the exposed scarp are compared with smooth terrain above the crater rim, and with Cannutia crater below the scarp. The plateau beyond the rim is called the Rheasilvia smooth terrain. The Rheasilvia basin is made up of ridge-and-groove terrain as described by (Krohn et al. 2014) and shown in Fig. 3. It plunges to depths of 12 to 13.7 km below the mean geoid (Fig. 2). There are six major and well-defined craters (Table 1), each with different morphological structures (Fig. 1) and colors (Fig. 4) that are examined with respect to their mineralogical surface composition in this paper. Are there spectral differences in the floors, walls and crater rims that tell a story about Vesta's history?
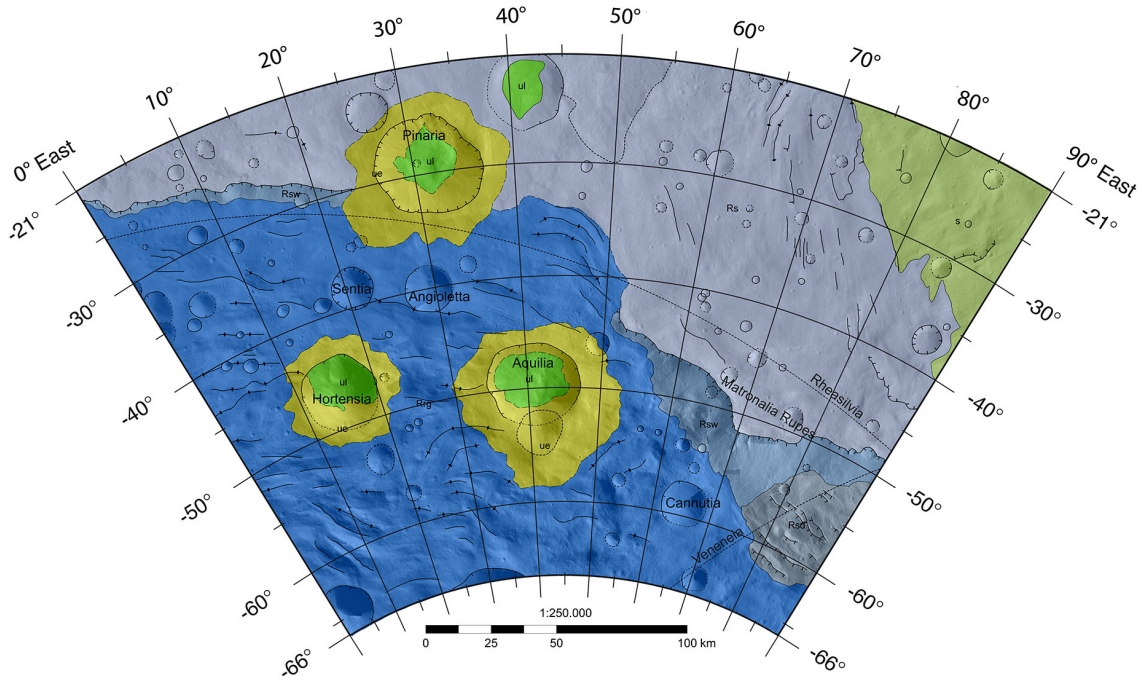
[Fig. 3 Geological map of Pinaria quadrangle from Krohn et al. 2014 with six defined terrains: (R stands for Rheasilvia), Rs, smooth terrain (violet), Rsw, scarp wall material (light blue), Rrg, ridge-and-groove terrain (dark blue), s, smooth material (pea green), ul, undifferentiated lobate material (green), ue, undifferentiated ejecta material (yellow-green).]

The largest crater is Pinaria, 42 km in diameter and located at 30°S, 32°E. The rim of Pinaria is almost coincident with a portion of the Rheasilvia rim, yet both are intact at this location. Aquilia (50°S, 41°E), 36.8 km in diameter, has a failed or breached wall on its southern rim. Next in size is Hortensia, 29.5 km in diameter (46.6S, 15.3E). It lies on the ridge-and-groove terrain, as does Aquilia. Yet, here we will show that the regolith composition of Hortensia is lower in diogenitic component than Aquilia. Sentia and Angioletta are both <20 km in diameter. Krohn et al. (2014) (Fig. 3) note a ridge crest very near the rim of Angioletta crater. The sixth crater studied, Cannutia, also <20km diameter, lies beneath the Rheasilvia scarp wall of Matronalia Rupes (Fig. 1), and we will show how its regolith composition is dominated by material slumped from the wall.

Table 1-Major craters in Pinaria Region

Crater	Lat-Claudia	Long-Claudia	Diam	Depth	IAU lat	IAU long
Pinaria	30S	31.6E	41.76	4.7	-29.54	181.63
Sentia	38.4S	20.7E	16.54	3.18	-38.39	170.75
Angioletta	40.0S	29.2E	18.42	4.97	-40.16	179.25
Hortensia	46.6S	15.3E	29.45	7.28	-46.85	165.38
Aquilia	50.1S	41.1E	36.82	7.42	-49.41	190.88

5

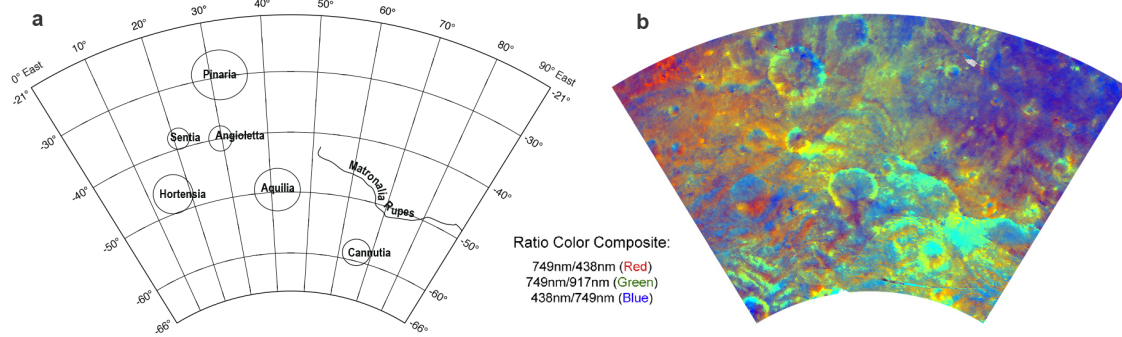|						
Cannutia	59.2S	65.0E	17.97	2.71	-58.93	214.73

Fig. 4a: Schematic showing the morphological features referenced in this paper. b:Ratio color composite map of VIR channels 0.749 μm/0.438 μm (Red), 0.749 μm/0.917 μm (Green), 0.438 μm/R0.749 μm (Blue).

In Fig. 4b the different colors associated with geomorphology motivates the analysis of VIR spectra to test the hypothesis that the features standing out in color ratios in the visible spectral region may correspond to mineralogical differences associated with crater rims, walls and floors and the different terrains and structures within this quadrangle. The examination of spectra and their absorption band parameters, presented here, build upon the geological mapping carried out by Krohn et al. (2014), color and albedo variations reported by Reddy et al. (2012), McFadden et al. (2012) and LeCorre et al. (2013), and elemental maps reported in Prettyman et al. (2012, 2013). Additionally, we assume that the relationships between spectral features and albedo presented by McCord et al. (2012), and Li et al. (2012) are valid for bright and dark features in the Pinaria region. We examine visible and infrared spectra of geologically distinct regions within the Pinaria quadrangle, in order to identify evidence of compositional variations interpreted from absorption band parameters, and to find their relationships to mineral compositions. We look for evidence of the manifestation of Vesta's interior composition exposed on the surface, or evidence of exogenic processes, such as mixing from impacting projectiles, to reveal processes forming the geological features in this region of Vesta. Our goal is to place the history of this region in context with Vesta as a tiny terrestrial planet.

2. Data Sets and Approach

Our analysis focuses on spectra returned from the Visible and Infrared Spectrometer (VIR) consisting of more than 850 spectral channels from the ultraviolet (UV) to the infrared (IR), between 0.25-5.1 μm (DeSanctis et al. 2011). We build upon the first results reported by DeSanctis et al. (2012a, 2013) and Ammannito et al. (2013), with the objective of examining more closely the spectral features in this quadrangle, as they relate to morphology, geology and chemistry, in order to determine what the surface composition tells us about Pinaria's regional history.

2.1. Examination of individual data cubes

VIR data were collected at three different altitudes, survey, high altitude mapping orbit (HAMO) and low altitude mapping orbit (LAMO). We first examined spectra in VIR cube 365900707, covering the crater Pinaria (Fig. 5). Reflectance spectra of Vesta are dominated by three spectral features, characteristic of the spectrally distinct Howardite-Eucrite-Diogenite (HED), basaltic achondrite meteorites (Gaffey, 1976). Vesta spectra include a UV charge transfer absorption band, and 1- and 2- µm spin-allowed absorption bands that are found in spectra of pyroxene minerals. Stephan et al. (2014) noted the weak spin forbidden band in the 505 nm region that can be used as a probe of iron mineralogy in pyroxenes on Vesta. In the 3-µm region, changing transmittance of order-sorting filters beyond 2.5 µm (DeSanctis et al. 2011) has been carefully calibrated by Combe et al. 2015. A weak and ubiquitous absorption has been reported at 2.8 µm and has been identified as an OH-bearing material (DeSanctis et al. 2012b, Combe et al. 2015 this issue). We present and discuss a map of the Pinaria region displaying 1.4 µm reflectance, the peak in Vesta's reflectance and the 2.8 µm band depth (Fig. 10).
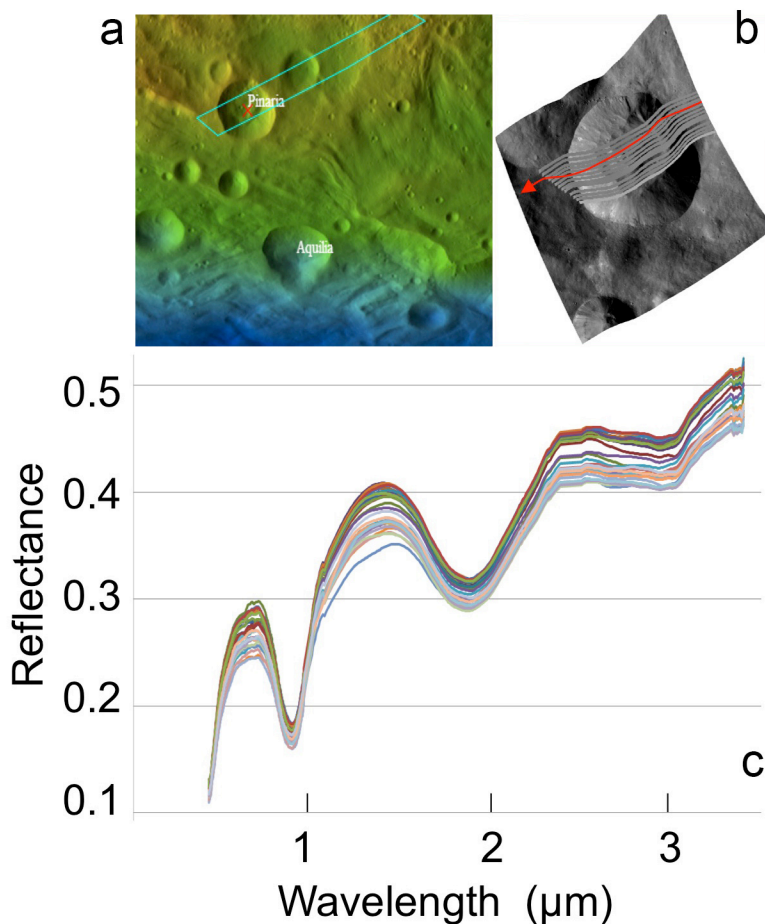
[Fig. 5: Study of Pinaria crater from portion of the radiometrically calibrated VIR cube 365900707. a: Topography map showing cube footprint. b: Framing Camera clear image with parallel lines representing part of the VIR footprint. The red arrow

marks the region of the crater from which a spectrum at each position along the line is plotted in (c). For the record they are spectra of samples 178-244 of the cube and the direction of the arrow is that of increasing sample number. c: Spectral reflectance differences in intensity of spectra from the rim, crater wall and floor with spectra at the bottom of the stack beginning at the right of the red arrow. Reflectance variations range from 10-17% at different segments of the spectrum. This plot shows the necessity of using band parameter maps for compositional interpretations as shifts in band position and depth are subtle and interpretation of reflectance outside of bands is ambiguous.]

2.2. Band parameters: calculation and interpretation

To optimize the information extracted from Vesta's spectra, we build upon the absorption band relationships derived by Adams (1974), which demonstrate that the band positions in the 1-µm (band 1) and 2-µm (band 2) region and their corresponding band depths are correlated with chemical mineralogy. This relationship was applied to Vesta (McCord et al 1970) when it was first associated with basaltic achondrite meteorites. Gaffey (1976) demonstrated that the band position and strength of reflectance spectra of HED meteorites are unique among known meteorite types. McFadden et al. (1982), Mayne et al. (2010), Mittlefehldt et al. (2011) studied the systematic relationships of many of the HED meteorites and a paper by Klima et al. (2010) examines these relationships from spectra of synthetically produced pyroxenes. More recently, in Moriarty & Pieters (2015) the absorption band relationships of synthetic pyroxenes are compared with HEDs showing small shifts in band position between the two (Fig. 6). It is with this wealth of laboratory spectral data and because the collected spectra of the Dawn spacecraft at Vesta number ~20 million, that the Dawn team decided to derive band parameters, centers and depths, that are the basis of interpretations of VIR spectra within the basaltic achondrite or HED paradigm (DeSanctis et al. 2014, Ammannito et al. 2013).

Futhermore, VIR data were collected under conditions of multiple viewing angles, combinations of incidence and emission angles that correspond to time of day of the observations and the spacecraft's position over Vesta relative to the sun, resulting in observations at different phase angles. With changes of incidence angle the temperature of the material changes and there is a small shift in band center, as reported by Hinrichs et al. (2002). Ruesch et al. (2015) using measurements of HED meteorites at different incidence and emission angles in the laboratory reported changes in slope and band depth and Longobardo et al. (2014) explored the dependence of phase angle on band parameters with Dawn spectra and performed photometric corrections on band depth values. Changes in band 1 center resulting from different phase angles are within measurement uncertainty of the data (Longobardo et al. 2014, Ruesch et al. 2015,). And the shift in band centers related to incidence angle, thus temperature, is smaller than the wavelength sampling interval of the VIR spectrometer. Band depths for both the 1- and 2-µm bands have been photometrically corrected as reported in Longobardo et al. (2014) (see section 2.3).

Fig. 6 shows the relationship of the position of the 1-µm vs. 2-µm bands measured in the Pinaria region compared to laboratory spectra of both synthetic pyroxenes and HED meteorites. We use the relationship between band centers to determine pyroxene chemistry and to look for evidence of olivine in the Pinaria region. Its presence would be shown in the position of the 1-µm band center being at longer wavelengths relative to the 2-µm band position along the pyroxene trend. This occurs when abundant olivine is present because there is no 2-µm band in olivine that consists of a three-band complex in the 1-µm region (e.g. Cloutis et al. 1986). Band centers derived from spectra in the Pinaria region span the range of those measured from HED meteorite reflectance spectra with most spectra falling in the howardite range.
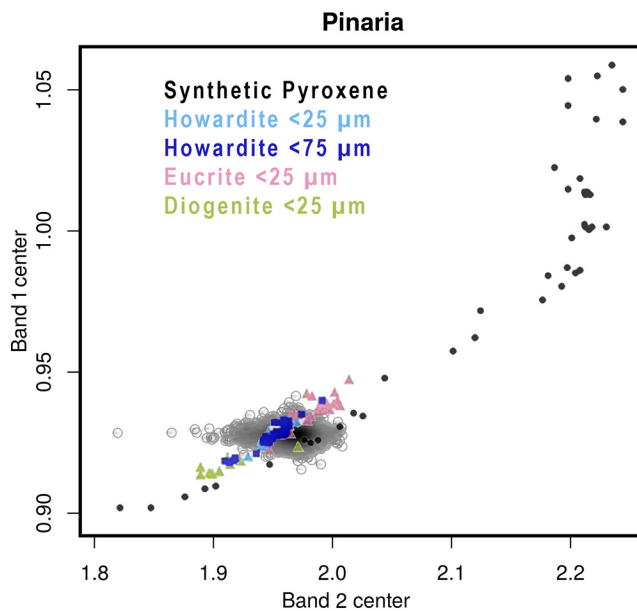

[Fig. 6: 1-µm vs. 2-µm band center positions of Pinaria quad spectral parameters (black-gray cloud), synthetic pyroxenes (black circles) (Klima et al. 2010), howardites <25 (cyan triangles) and <75 µm (blue squares) characterized by Mittlefehldt, Eucrites (pink triangles) and Diogenites (green triangles) from Burbine et al. (2001). Compiled lab data from Moriarity & Pieters, 2015).]

2.3. Spectral Maps

Band parameter maps of radiometrically and photometrically calibrated band 1 and band 2 centers are presented in Fig. 7a, c. The band 1 and 2 band depths have been both radiometrically calibrated (Frigeri 2015) and photometrically corrected by Longobardo et al. (2014) in Fig. 7 b,d. The production of these maps is described and presented in Frigeri et al. (2015). We use these maps to explore the relationship between morphological and geological features in Pinaria region and mineral composition as found across the HED range of meteorites. From the results we offer possible scenarios for the observed distribution of HED-types in both spatial and time dimensions. In Fig. 7 a, c, the blue regions have band centers at shorter wavelength indicative of low-iron, low-ca orthopyroxenes. The longest wavelengths represented in red, represent the average of

9

both low-ca pyroxene and more calcium-rich clinopyroxene found in eucrites. The band depth maps, Fig. 7b, d have shallow band depths shown in blue, and the highest in red. The band depths represent combinations of chemistry and grain size that can be difficult to disentangle. We discuss the association of these parameters with specific regions in Pinaria in section 3.
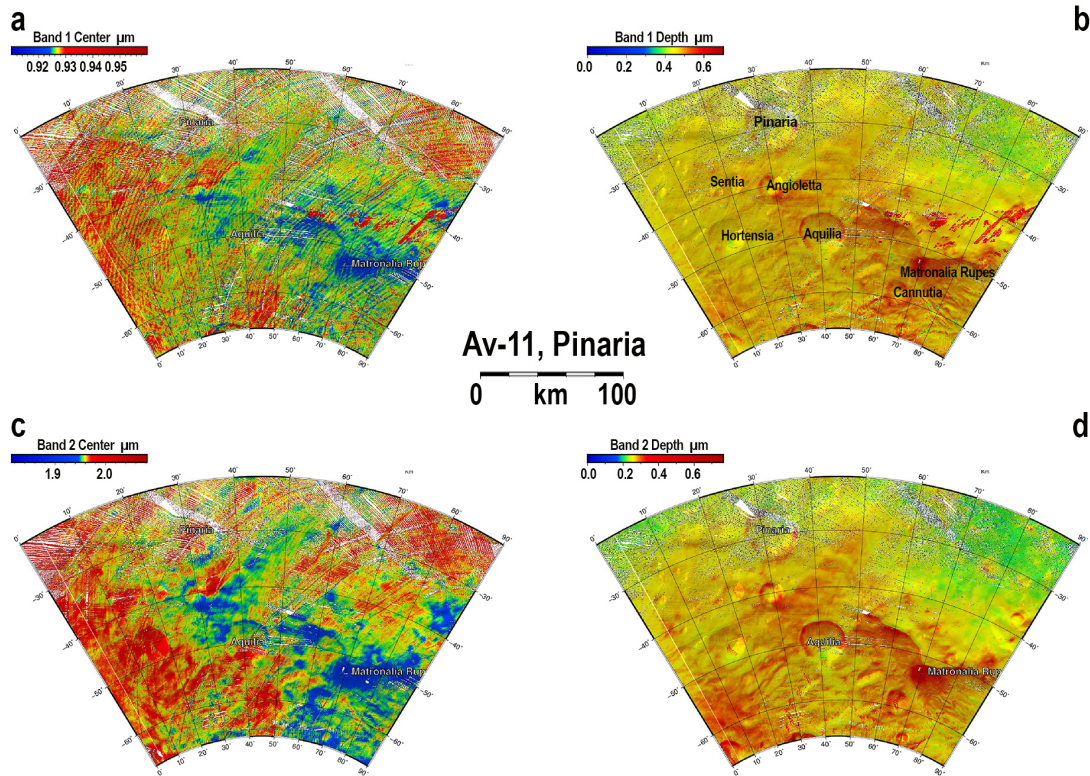
[Figure 7: Band parameter maps derived from radiometrically corrected spectra shown in Lambert projection (Frigeri et al. 2015 this issue).]

In Fig. 8a, the band 1 and 2 center parameters of Fig. 7a,c (Frigeri et al. 2015, this issue) are plotted as gray-to-black values depending on their frequency of occurrence. Light gray values don't occur as frequently as black values and each gray-black value represents a location within Pinaria. These values are plotted over a two-dimensional color table organized around red, yellow and blue primary colors that is close to the standard Red-Green-Blue subset of colors developed for use on monitors, printers and the internet and allows for representation of a large combination of contrasts and colors. We then convert each value in Fig. 8a to the corresponding color in the color table and map each value to the latitude and longitude position within Pinaria region in Fig. 8b. Interpretation of these colors in terms of mineralogy and HED type comes from comparing the band-band values in Fig. 6 for HED meteorites. The regions mapping in magenta are more diogenite-rich regions, yellow and green-blue regions are howardite assemblages, and bright green regions are more eucritic.
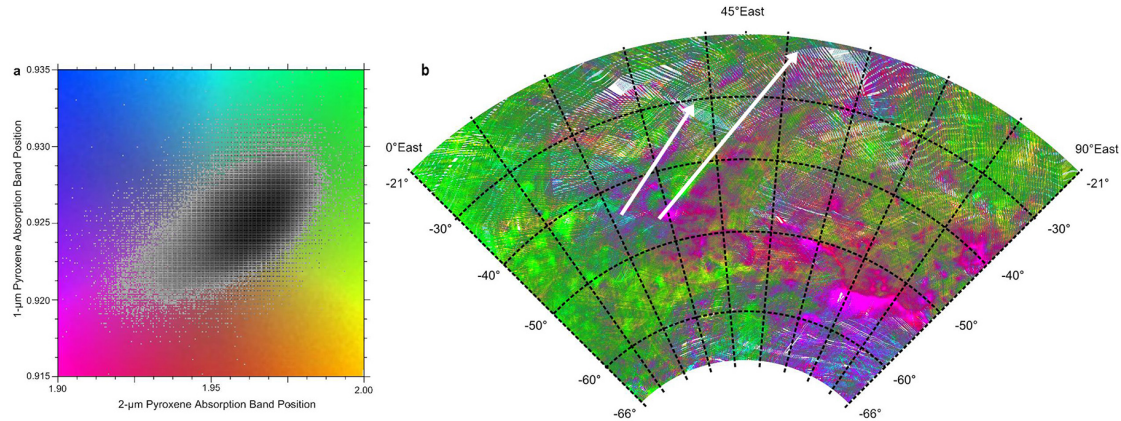
[Figure 8a: Band 1 center vs. Band 2 center values plotted in gray-to-black depending on frequency of their occurrence in the Pinaria region. The background color palette serves as a legend for the map in b, where each value is assigned the corresponding color from the background palette and mapped to its location in Pinaria. Arrows outline two lanes of diogenite-rich material discussed in Sec. 3]

In Section 3 we examine the band centers and depths of spectra associated with major craters. In some cases, their interior and surrounding regions have different spectral parameters, indicative of relative compositional differences, in others there is no variation. We also explore and interpret the composition of the ridge-and-groove terrain of the Rheasilvia basin, the scarp of Matronalia Rupes, and the smooth plains north of the basin's rim.

We also make use of a global bidirectional reflectance map at 1.4 µm (Fig. 9, Combe et al. 2015, this issue) presented at 30° phase angle (with incidence angle of 30° and emergence angle of 0°). Photometric corrections using the Akimov disk and Shkuratov phase function have been applied to minimize the effects of topography. The reflectance at this wavelength is a first line indicator of whether the material is HED-like or not. Vesta at the global scale and Basaltic Achondrite meteorites both have high reflectance at this wavelength because of their mineral composition, crystalline nature, and absence of light-absorbing, opaque material. This is a useful parameter for constraining the amount of dark material in the Pinaria region and is discussed further in section 3.
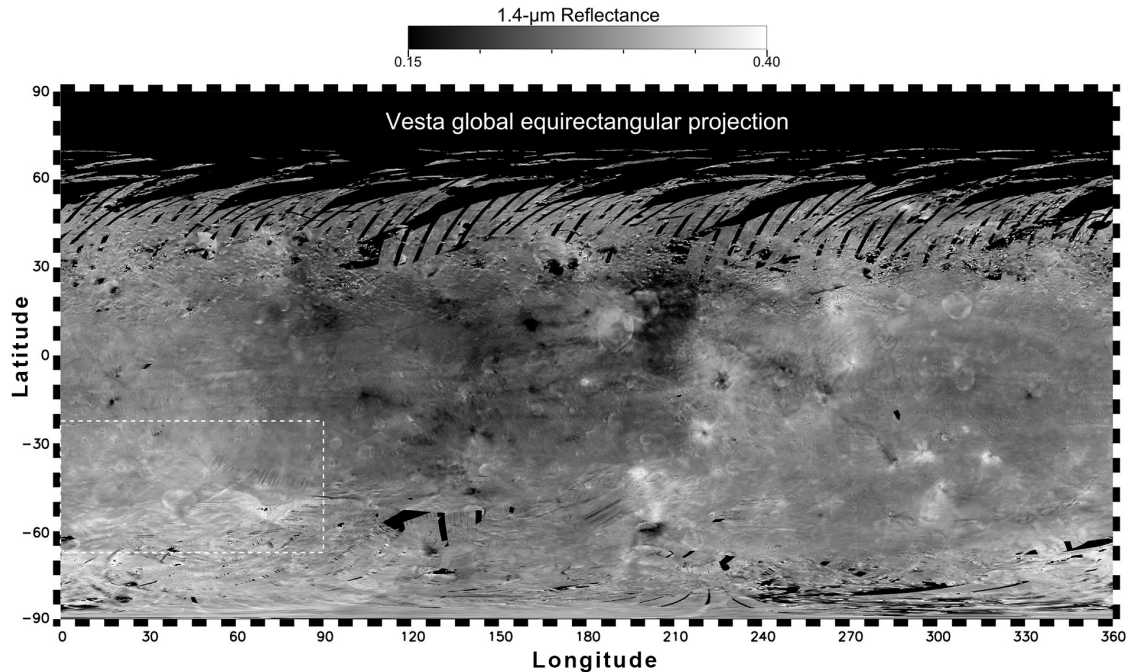
[Figure 9: Reflectance map of Vesta at 1.4 μm – Pinaria quadrangle outlined in dashes at Southeast of the map displayed in Claudia coordinates shows that Pinaria is among the brightest regions of Vesta.]

Fig. 10a shows the photometrically corrected reflectance at 1.4 μm versus depth of the 2.8-μm band (Combe et al. 2015) plotted on a scale relative to the range observed across all of Vesta. The values in the scatter plot are converted to the background color palette and used to map the values as a function of position (lat-long) onto the Lambert projection of the region (Fig. 10b). The color palette is chosen to enhance contrasts between brightness and 2.8 μm absorption depth. In this map cold colors, such as blues and greens, are associated with deeper 2.8 micron absorption and thus relatively more hydrated materials while the warm colors represent areas of less hydrated material. Yellow regions are highly reflective and lack OH absorption and red-magenta regions are less so.

2.4. 3D display of photometrically corrected cubes

Fig. 11 and 12 are 3D projections of photometrically corrected image cubes, using coefficients calculated by Li et al. (2013). The data are overlaid onto clear filter Framing Camera images to enhance the relationship between topography and mineralogy. Below we address the band center ranges for band 1 (Fig. 7a), band 2 (Fig. 7c) and refer to the HED assemblage derived from locating these parameters on Fig. 6. Then the association of band centers is noted for crater components: floor, wall, rim and surrounding areas. Band depths are noted from Fig. 7b and 7d. We then look for an association of band parameters with geology or topography by comparing band parameter maps with Fig. 1, 2 and 3.

3. Results

3.1. Albedo and Reflectance at 1.4 µm

The albedo of the Pinaria region at 0.750 µm (Reddy et al. 2012) and the 1.4 µm reflectance (Fig. 9) shows this region to be among the brightest of Vesta's regions. The southern portions of the adjacent quadrangles to the north, Gegania and Lucaria (Longobardo et al. 2015, this issue) are also bright. McCord et al. (2012) and Palomba et al. (2014) find no dark areas in Pinaria. Typically, high albedos may be intrinsic to surface composition (large single particle scattering albedo); may indicate the absence of a low albedo component; and/or indicate the presence of many grain boundaries. Longobardo et al. (2015, this issue) conclude that grain size in both bright and dark material in Gegania and Lucaria quadrangles is the same. Palomba et al. (2014) found over-all homogeneity in grain size across Vesta. Because the southern portions of Gegania and Lucaria are similar to the northern portion of Pinaria, they are of the same mineralogical province. Thus, we conclude that high single particle scattering albedo and low abundance of dark material are responsible for the high reflectance of the Pinaria region.

3.2. 2.8 µm band

Fig. 10a shows that high reflectance at 1.4 µm in Pinaria region is correlated with a low value of the 2.8 µm absorption band. The distribution of reflectance vs. band depth in Pinaria is plotted with axes spanning the values of these parameters observed on Vesta globally in Fig. 10b. In the Pinaria region, the high reflectance implies small amounts of dark, OH-bearing material an interpretation that is also supported by the low 2.8 µm band depth (DeSanctis et al. 2012 and Combe et al. 2015, this issue). The spectrum in Fig. 5 of the Pinaria crater shows a weak absorption at 2.8 µm, and the Pinaria region in general remains one of the least hydrated regions of the planet. With both high reflectance and low abundance of OH-bearing material, this region may be considered "the Pinaria desert".
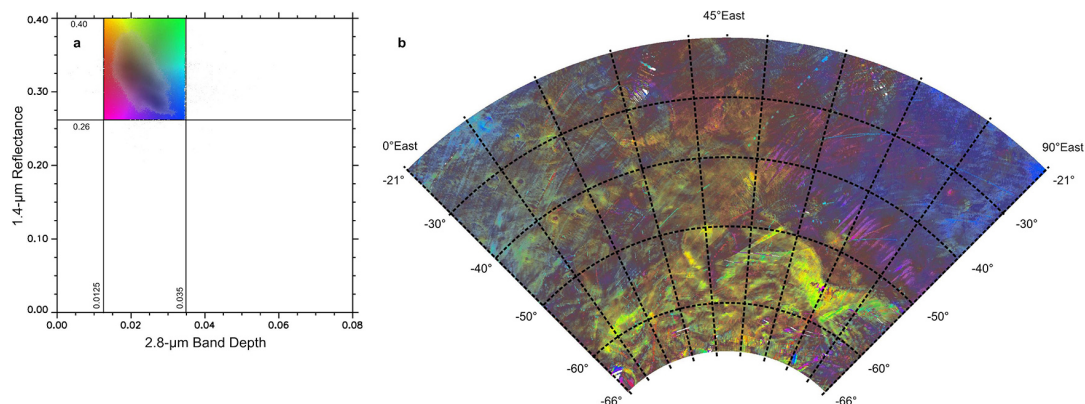
[Figure 10: a) Gray points are the scatter plot of 1.4 µm reflectance versus 2.8 µm band depth in Pinaria, where values occurring less frequently are shown in light gray, and those occurring more frequently are black. The values overly a color palette selected to

represent a large combination of contrasts and colors and serves as a legend for b) Map of the distribution of points shown in (a) with colors assigned from the background color palette displayed in a. The Pinaria region has high reflectance and weak 2.8 μm bands relative to the rest of Vesta.]

3.3. Absence of olivine

Examination of Fig. 6 shows that the greatest density of spectra in the Pinaria region falls within the howardite range of pyroxene composition and does not extend above that region that would suggest the presence of olivine. We further searched for evidence of the weak absorption feature around 0.6 μm found in olivine (Shestopalov et al. 2008), and found no evidence of it. This approach is effective when olivine is present in abundances >35-40%. Approaches to detect olivine in lower abundances have been developed by Reusch et al. (2014), Palomba et al. (2015) and Shestopalov et al. (2015) using olivine indices. As an example, three possible deposits of olivine were found and reported around the Lollia and Graecina craters (Reusch et al. 2014). Palomba et al. (2015), using a combination of two different olivine spectral indices did not detect any olivine-rich deposits in the Pinaria quadrangle. The Pinaria region lacks olivine and shows no signs of mantle-like material.

3.4. Spectral properties of major craters and geological terrain

1. Pinaria (30S, 31.6E; 41.76 km in diameter; 4.7 km deep)
In the clear filter image (Fig. 1), slumped material can be seen accumulated on the floor of Pinaria crater, with a small crater superimposed on it. This undifferentiated lobate material (Fig. 3), and the lower walls of the crater close to it are spectrally distinguished by having weaker absorption bands than material on the upper walls of the crater (Fig. 7 b,d). Linear artifacts associated with the track of the spacecraft are visible in the projection of the data in Fig. 7, and should be ignored. Band 1 centers range from 0.925-0.930 μm (green to red) and band 2 centers range from 1.96-1.98 μm (yellow-red) (Fig. 7 a and b). These positions are consistent with howardite mineralogy (Fig. 6). In Fig. 11, cube VIR_1B_1_372786228 is presented to illustrate the following interpretation. The upper wall of the southeastern portion of the crater is brighter than other regions (Fig. 10) and has longer wavelength band centers (yellow Fig. 11a) than most of the crater's interior. Just beyond the southeast rim, the material is more diogenite-rich (red Fig. 11c), because band centers are at shorter wavelengths relative to the crater material itself (Fig. 8, 11a). Band 1 depths range from 0.4-0.5 μm (yellow, Fig. 7b) and band 2 depths from 0.25-0.4 μm (yellow-red, Fig. 7 d). The upper walls of Pinaria crater have deeper bands near the crater rim than those observed on the crater floor (red-yellow, Fig. 11b, Fig. 7 b and d). The upper walls and rim area of Pinaria are more diogenite rich than the lower walls and crater floor. Below (Sec. 4) we discuss this compositional variation, along with observed thermal variations on the wall of Pinaria (Fig. 11b) reported by Tosi et al. (2014).
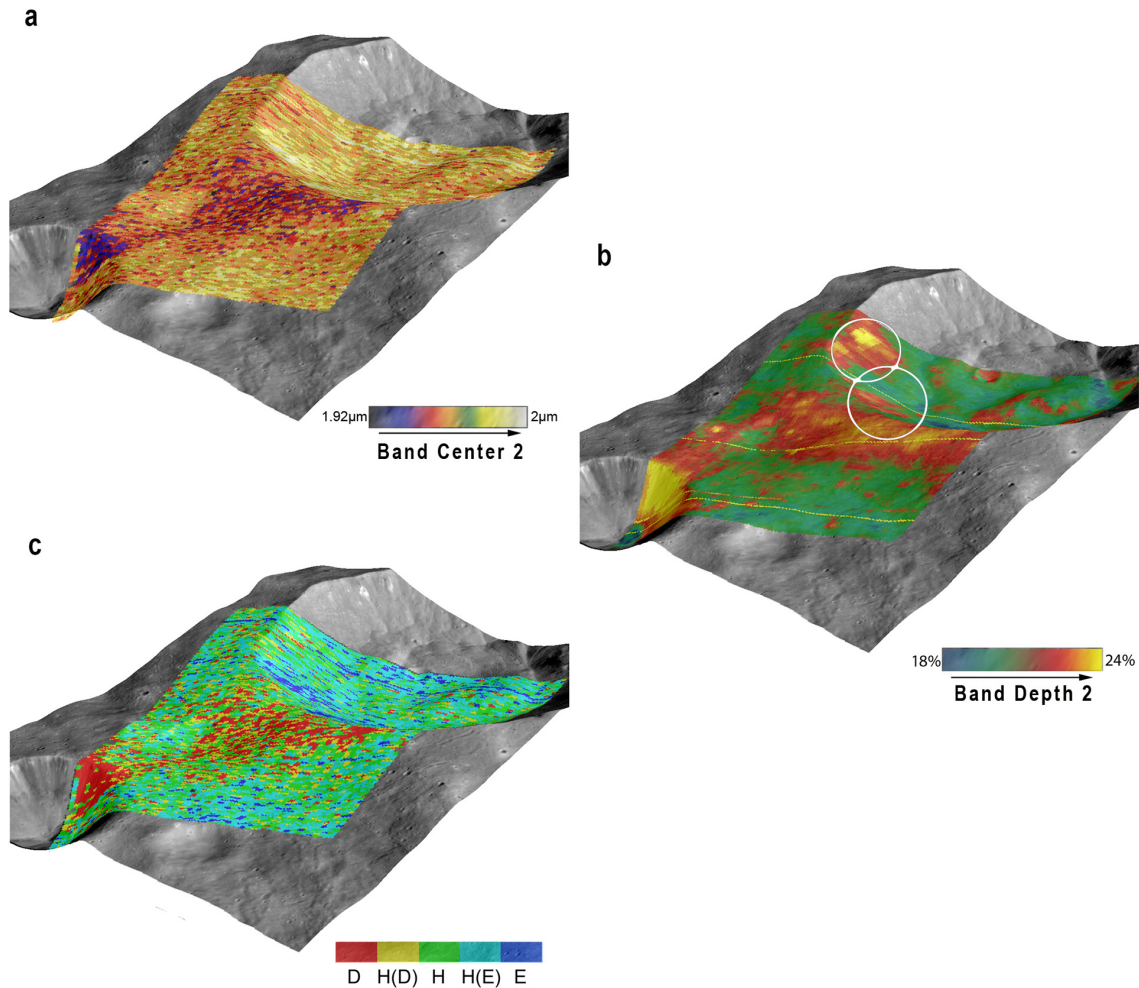
[Figure 11: Floor and western wall of Pinaria and eastern wall of Angioletta craters (cube VIR_1B_1_372786228). a: Band 2 center values overlayed on a corresponding FC clear filter image projected in 3D using a digital terrain model for coordinate projection. b: Band 2 depth, using the same display as (a). White circles are bright, cold spots reported by Tosi et al. 2014. c: Data are presented in terms of the range of band parameters representing basaltic achondrite HED types DeSanctis et al. 2012.]

2. Sentia (38.4S, 20.7E; 16.5 km in diameter km; 3.18 km deep)
Sentia appears to have erased the ridge upon which it formed (Fig. 1,2, 3). It is difficult to find in band parameter maps (eg. Fig. 7) suggesting little change in mineralogy between the floor, walls and rim of this crater that lies on top of Rheasilvia ridge-and-groove terrain (Fig. 3). Band 1 wavelength centers range from ~ 0.926-0.933 μm (yellow-red, Fig. 7a), and band 2 centers range from ~ 1.95-1.97 μm (yellow-red, Fig. 7c). In terms of HED band parameters, the Sentia crater's band centers are in the howardite region (Fig. 6). In Fig. 4, this crater is notable in comparison with others in Pinaria in that its rim is not defined by color differences and in band parameter space (Fig. 8b) it is essentially indistinguishable from the surrounding howarditic terrain. The range in band parameters is small across the floor, slopes and visually relaxed rim of this crater. It is also shallower

than its neighboring crater, Angioletta, suggesting that it is older and partially filled with impact ejecta of howardite composition.

3. Angioletta (40.0S, 29.2E; 18km in diameter; 4.97 km deep)
Angioletta crater formed between a ridge and the Rheasilvia crater wall (Fig. 1, 2, 3). The band 1 centers of crater Angioletta range from 0.923-0.925 µm (yellow-red, Fig. 7a) and band 2 ranges from 1.93-1.97 µm (green-red Fig. 7c). These band centers are also in the howardite range (Fig. 6). The distribution of visible colors (Fig. 4) and band parameters relative to the crater features is different at Angioletta compared to Sentia (Fig. 7, 8). Around Angioletta crater's rim, the band centers are at a shorter wavelength relative to the crater's walls and floor. This is also true of the band depths that are deeper around the crater rim than at the crater floor. These band depths occur in a concentric pattern around crater center, suggesting downward motion of material. This can also be seen in Fig. 11 where portions of the wall of Angioletta are on the diogenite side of howardites (red Fig. 11c) with shorter wavelength band 2 center (blue, Fig. 11a) and a deeper band 2 (yellow, Fig. 11b). Angioletta crater is deeper than Sentia and has a concentration of diogenite-rich howardite material on its southeastern rim.

4. Hortensia (46.6S, 15.3E; 28.0 km in diameter; 7.28 km deep)
Hortensia crater contains undifferentiated lobate material on its floor (Fig. 3) and has a higher north rim and steeper wall than its southern rim and wall (Fig. 2). Band 1 centers range from 0.926-0.94 (green-red Fig. 7a) and band 2 centers range from 1.965-2.03 µm (red, Fig. 7c). These are the longest band centers of any of the craters in the Pinaria region. They are thus compositionally on the eucrite end of howardite composition (Fig. 6). Band centers are mostly uniform across the crater floor, wall and rim (Fig. 8b). The band depths range from 0.4-0.5 at band 1 (yellow, Fig. 7b) and 0.25-0.4 at band 2 (yellow-red Fig. 7d). The band depths of both bands are more shallow than at the southern wall and rim, and are similar to the variation in Aquilia's band depth discussed next. A structural difference between Hortensia and Aquila is that the rim of Hortensia is intact, though in the clear filter map (Fig. 1), it appears more filled in or degraded than Aquilia. The difference in band 2 depth relative to band 1 depth between Hortensia and Aquilia craters can be explained by the addition of a second pyroxene in Hortensia material that is not present in Aquilia material.

5. Aquilia (50.1S, 41.1E; 36.8 km in diameter; 7.43 km deep)
The southern wall of Aquilia crater is breached (Fig. 1, 2 and 3) and visible color ratio in the breached wall area (Fig. 4) is different than its well-formed crater rim. The intact rim of the northern rim and wall has shorter band centers than its southern wall. Band 1 centers for the northern rim range from 0.922-0.925 µm (blue –yellow Fig. 7a) with most of the wall's centers at 0.925. Band 2 centers range from 1.92-1.95 µm (blue-yellow Fig. 7c). The HED composition of these band centers falls in the howardite-diogenite range (Fig. 6). The longest wavelength band centers in crater Aquilia are associated with the failed part of the rim and the material that flowed from it. Here the band centers fall on the howardite-eucrite of the HED pyroxene compositions (Fig. 6) relative to the rest of this crater (Fig. 7, 8a).

6. Cannutia (59.2S, 65.0E; 18.0 km in diameter; 2.71 km deep)

Cannutia crater lies deepest in the Rheasilvia basin compared to other craters discussed here (Fig. 1, 2). It contains no lobate material (Fig. 3) and can be identified in the color map (Fig. 4) as having a different visible colored floor compared to surrounding areas. Its band parameters are distinctive as described here. Band 1 centers range from 0.922-0.926 µm (blue-green Fig. 7a) while band 2 centers range from 1.93-1.95 µm (blue-green-yellow Fig. 7 c). These band centers are in the diogenite region of the band 1 vs band 2 plot (Fig. 6 and 8a). Band 1 depths are relatively high, in the range of 0.45-0.65 µm at band 1 (yellow-red Fig. 7b), and 0.38-0.45 at band 2 (yellow-red Fig. 7d), also indicative of a diogenite-to-howardite composition. There is a small variation in band 2 depth, with the shallower band 2 depth found on the southeast wall of the crater. Geographical differences in the distribution of band 1 depth versus band 2 depth in this crater are puzzling and may not be significant. While most of the pyroxene is diogenite in composition, the presence of a second pyroxene, indicating addition of a eucrite component, makes the composition howarditic. This second component likely came from mass wasting of the eucritic crust from the Rheasilvia smooth terrain, and/or from ejecta from a more distant impact.

3.5. What is the nature of the difference between the Rheasilvia smooth material and the Rheasilvia scarp material?

In Fig. 7 and 8, Matronalia Rupes is shown with band 1 and band 2 centers (fig. 7 a,c) that are the shortest wavelengths seen in the Pinaria region, and indeed for all of Vesta (DeSanctis et al. 2012). The absorption band depths are also large for both bands (Fig. 7b and d). With short wavelength band centers, and deep absorption bands, the dominant mineralogy is orthopyroxene (e.g. Adams, 1974), and the meteoritic analogue is that of diogenites (Fig. 6). We display the band centers and band depths of a cube containing the Matronalia Rupes scarp in 3-D projection on top of a clear filter image in Fig. 12a, b. The association between the band position and depth Fig. 12c shows the color scale used by Ammannito et al. (2013) to represent HED pyroxene compositions. The scarp shows exposed diogenite and further downslope of it there is material with band position at longer wavelength (Fig. 11a). This suggests that the diogenite material exists beneath a layer of eucrite material that has traveled down-slope (Fig.11c). Smooth plains material above the scarp has regions of band 1 centers between 0.925-0.94 µm (green-yellow-red Fig. 7a) and band 2 centers ranging from 1.95-2.0 µm (green-yellow-red, Fig. 7c). On the band-band plot (Fig. 6 and 8), these band positions are shown to arise from the presence of low-Ca orthopyroxenes characteristic of diogenites and pigeonites, low-iron clinopyroxene that are characteristic of eucrite meteorites.

The longer wavelength band centers of the Rheasilvia smooth plains close to the scarp indicate a diogenite-howarditic composition, in comparison to the scarp that is predominantly diogenite. The Rheasilvia smooth plains contain more dark hydrated material than elsewhere in the region (blue, Fig. 10b). This is confirmed by examining Fig. 9 where the southwestern portion of the dark hemisphere extends into the northeast region of Pinaria. Away from the scarp rim, the smooth material contains more eucritic pyroxene composition according to the maps (Fig. 6, 7, 8).
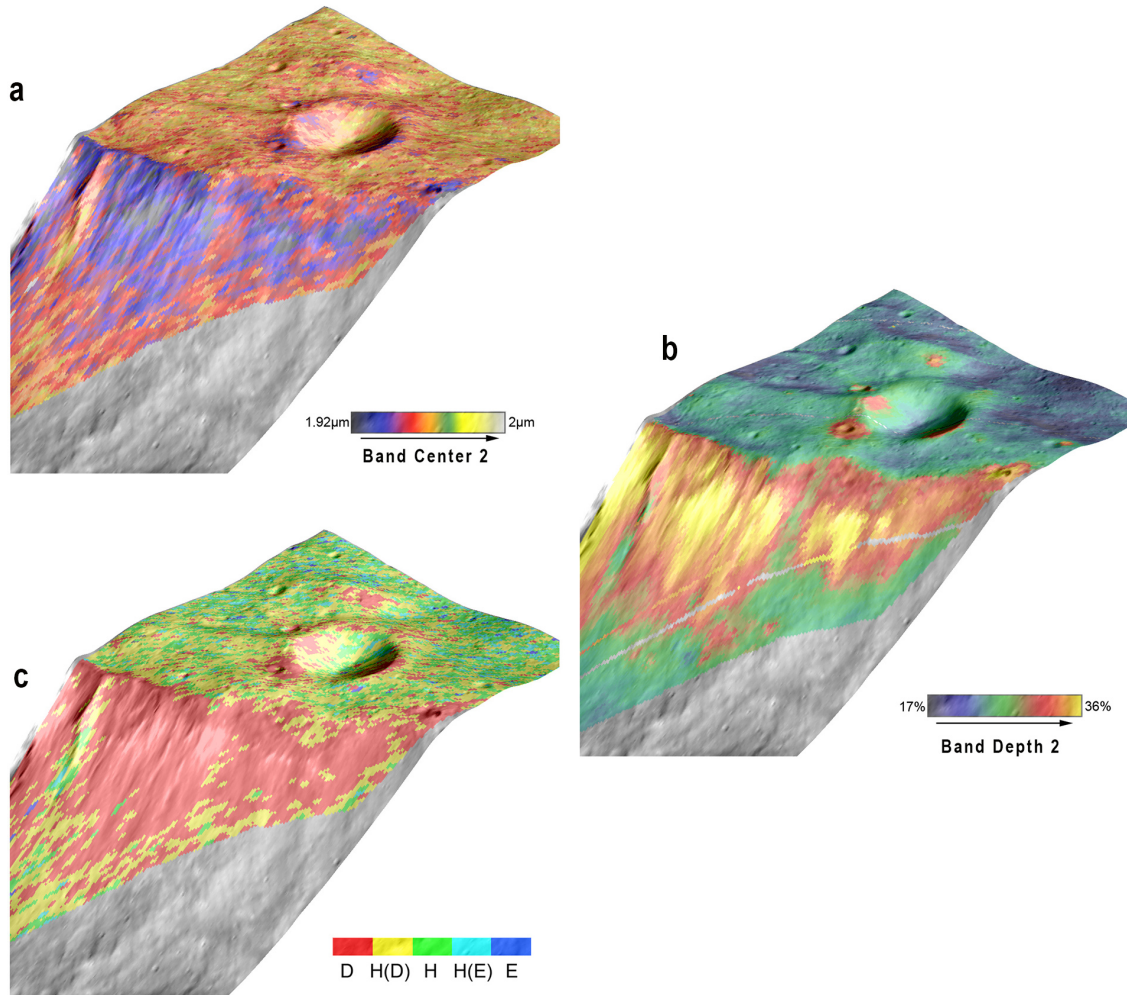
[Figure 12: Matronalia Rupes scarp. a: absorption band position of the 2-micron band on the Matronalia Rupes scarp draped over a clear image projected onto the 3D projection of the digital terrain model. b: absorption band depth of the 2-micron band on the Matronalia Rupes scarp in the Pinaria region. The deep band (yellow) is located spatially where the band position is at shortest wavelength for the Pinaria region. c: Combining the band positions using the color schematic discussed in Ammannito et al. 2013 to display HED composition ranges.]

Other areas in Pinaria with diogenite-rich material extend around the north rim of the crater Aquila and the ejecta extending south and east of the crater Angioletta, as well as at the crater's northeast rim (Fig. 8b, Fig. 10b). Assemblages with these band parameters are considered diogenitic because diogenite meteorites are dominated by orthopyroxene with low iron and low calcium.

The last area to note in Pinaria is the western edge of the region that we characterize as howardite with a more eucritic composition. In this region the band 1 centers range from 0.925-0.945 (green-yellow-red, Fig. 7a) and band 2 centers range from 1.96-2.0 (yellow-red, Fig. 7c). These indicate pyroxenes in the howardite-eucrite range. Fig. 9 shows the

material is bright and fig. 10 indicates that it is bright and has a weak 2.8 μm absorption band from which we conclude that there is very little hydrated material, consistent with the assignment of this region as relatively desert-like.

4. Discussion

The Pinaria region is part of Vesta's brighter hemisphere, known from ground-based observations (Gaffey 1997). Our analysis in this paper shows that Pinaria is the region of Vesta that is brightest and least hydrated, hence its reference as the Pinaria desert. The dark, hydrated material that produces Vesta's dark material units, and creates the two wide dark areas on Vesta (McCord et al. Nature 2012; Palomba et al. 2014), is seen in small amounts in the northeast corner of the region. In this sense, Pinaria is mostly original, relatively uncontaminated basaltic achondrite material. It is likely where howardite material formed from mixing of Vesta's upper, eucritic crust, with its lower, diogenitic crust as a result of crater impacts.

Having established that the Matronalia Rupes scarp is diogenitic material, and that the smooth plains above it is on the diogenite-howardite-eucrite trend with increasing distance from Matronalia Rupes, it is reasonable to consider why other regions in Pinaria have exposed diogenitic material. Referring to Fig. 7, diogenitic compositions exist in regions designated by the color magenta: (1) on the walls and rim of Cannutia crater; (2) on the upper walls, near the rim of Aquilia crater; (3) on the south east region beyond the rim of crater Angioletta; and (4) beyond the rim of Pinaria crater. Cannutia crater is in the Rheasilvia basin, on the ridge-and-groove terrain (Fig. 3) and is diogenitic material as expected because Rheasilvia basin itself is diogenite-rich (Ammannitto et al. 2013). The projectile forming Aquilia crater impacted on a slope in the Rheasilvia basin and as Krohn et al. (2013) discuss, the mass wasting process of material at higher elevation, sliding to lower elevations would account for the more eucritic material sliding into regions of lower elevation. The result is, again, a howardite composition, which implies mixing of eucrite and diogenite. The absence of dark material, or other non-basaltic material, support this theory.

Looking at the clear filter topographic map (Fig. 1), we see Angioletta crater sitting in ridge-and-groove terrain to the north and west. The crater is on a terrace of the Rheasilvia basin. This crater too shows diogenitic material with superimposed howardite-eucrite material, both in the crater's center and extending up its eastern slope and onto a regional high elevation extending north and east. The source of the howardite-eucrite rich material is difficult to explain from examining Pinaria region alone. Its source is likely beyond Pinaria.

The projectile creating the Pinaria crater landed on the rim of the Rheasilvia basin and the crater is mostly within the Rheasilvia smooth plains (Fig. 3). The surface composition of Pinaria falls on the howardite-eucrite continuum. Material surrounding Pinaria crater is shown in Fig. 2 to be at high elevation, although not as high as Matronalia Rupes. The occurrence of diogenitic material beyond the Pinaria crater rim suggests that it is remnant material from the Rheasilvia basin associated with uplifted material from the Rheasilvia

impact event. Presumably, if one could excavate to the bottom of Pinaria crater, the deepest part would also be diogenite-rich. The accumulated material in the bottom of the crater could be ejecta from an impact outside of the Pinaria region, or mass wasted material from the Pinaria impact.

Tosi et al. (2014) observed that the southwest wall of Pinaria crater has two bright and cool spots that we locate in Fig. 11b. Their observations are based on thermal IR variations related to the observation's time of day. The observed compositional variations across the Pinaria crater (Fig. 11 a-c) cannot explain the thermal differences, and we conclude that a physically compact region with less regolith cover best explains the thermal observations. The thermal inertia of pyroxenes of different composition cannot explain the observed thermal variations.

The Hortensia projectile impacted the Rheasilvia basin on ridge-and-groove terrain, as did Aquilia-forming projectile. Hortensia is smaller than Aquilia, yet the band centers of Hortensia crater are at longer wavelengths than Aquilia, indicative of howardite-eucrite compositions as is the entire western region of this quadrangle. It is possible that ejecta from the Urbinia or Oppia quadrangles extends into Pinaria. Likewise, crater Sentia is on the same terrace as Angioletta (Sentia is slightly smaller than Angioletta), yet there is no evidence of diogenitic material associated with Sentia. If diogenite were exposed at the surface, it has been covered up as a result of the Sentia impact. We propose that there is an ejecta ray of diogenitic composition trending from southwest to northeast passing between Sentia and Angioletta craters.

Prior to arriving at Vesta, we expected the entire Rheasilvia basin to be diogenite with a possibility of a detectable olivine component, from exposed mantle (Gaffey et al. 1997, Binzel et al. 1997). Instead, the Rheasilvia basin appears to be filled with regolith that is a mixture of impact ejecta formed subsequent to the formation of Rheasilvia basin. Both altimetry and high resolution image cubes (Fig. 2 and 12) of this region show that the steep slope of Matronalia Rupes is exposed and devoid of regolith. It's altitude relative to the mean geoid tells us that it is uplifted and the physics of basin formation (Melosh, 1989), points to its occurring during Rheasilvia's formation. This suggests that we are seeing the uplifted rim of the basin and thus a lower portion of a layered crust as proposed by Takeda et al. (1979) and discussed also in Mittlefehldt et al. (2011). The absorption band parameters and implications for surface composition support this scenario. Pinaria is bright and anhydrous relative to the rest of the asteroid. There are compositionally distinct diogenite-rich lanes or rays that are not coincident with morphology, topography, or albedo alone. Compositional trends of pyroxenes, considered along with topography and crater morphology, reveal ejecta patterns from multiple impact events, some of which exposed Vesta's original lower crust.

5. Conclusions and Summary
The results tell us the following:
1. Two lanes of diogenite-rich regolith trending from southwest to northeast is observed between Angioletta and Aquilia craters. This material is predominantly

diogenite-rich regolith bounded by howardite-eucrite material and lies on top of, and does not follow, local topography.

       2. The exposed scarp of Matronalia Rupes is dominated by low-Ca pyroxene, which is diagnostic of diogenitic material, while the smooth terrain above the rim has a more eucrite-rich composition with a discernible diogenite component.

       3. The Pinaria region lacks olivine and shows no signs of mantle-like material.

       4. Compared to Vesta on a global scale, the Pinaria region is bright and the presence of water is minimal. It is in effect one of Vesta's 'desert regions', dominated by howardite-like regolith that varies from diogenite-rich to eucrite-rich. The source of eucritic material in the Rheasilvia basin is partially from down-slope mass wasting plus mixing from ejecta of post-Rheasilvia impacts.

       5. Within the Pinaria crater, the regions of lower thermal inertia cannot be explained by composition alone and are likely, as concluded by Tosi et al., caused by a structure of different thermal inertia within the crater and not due to a compositional difference.

References

Adams, J.B. 1974. Visible and near-infrared diffuse reflectance spectra of pyroxenes as applied to remote sensing of solid objects in the solar system. J. Geophys. Res. 79, 4829-4836. DOI: 10.1029/JB079i032p04829

Ammannito, Eleonora, M. Cristina De Sanctis, Fabrizio Cappacioni,
M. Teresa Capria, F. Carraro, Jean-Philippe Combe, Sergio Fonte,
Alessandro Frigeri, Steven P. Joy, Andrea Longobardo, Gianfranco Magni,
Simone Marchi, Thomas B. MCCord, Lucy A. MCFadden, Harry Y. MCSween,

Ernesto Palomba, Carle M. Pieters Carol A. Polanskey, Carol A. Raymond,
Jessica M. Sunshine, Federico Tosi, Francesca Zambon, and Christopher T. Russell
Vestan lithologies mapped by the visual and infrared spectrometer on Dawn Meteoritics
& Planetary Science 1–14 (2013)
doi: 10.1111/maps.12192

Binzel, R.P., Gaffey, M.J., Thomas, P.C., Zellner, B.H., Storrs, A.D., Wells, E.N., 1997.
Geological mapping of Vesta from 1994 Hubble Space Telescope images. Icarus
128, 95–103.

Burbine T. H., Buchanan P. C., R. P., Bus S. J., Hiroi T., Hinrichs J. L., Meibom
A., and McCoy T. J. 2001. Vesta, Vestoids, and the howardite, eucrite, diogenite
group: Relationships and the origin of spectral differences. Meteoritics & Planetary
Science 36:6:761-781.

De Sanctis, M.C., A. Coradini, E. Ammannito, G. Filacchione, M.T. Capria, S. Fonte, E.
Magni, A. Barbis, A. Bini, M. Dami, I. Ficai-Veltroni, G. Preti, the VIR team (2011). The
VIR spectrometer. Space Sci. Rev., 163 (2011), pp. 329–369

De Sanctis, M. C., et al. (2012a), Spectroscopic Characterization of Mineralogy and Its
Diversity Across Vesta, *Science*, *336*(6082), 697-700.

De Sanctis, M. C., et al. (2012b), Detection of Widespread Hydrated Materials on Vesta
by the VIR Imaging Spectrometer on board the Dawn Mission, *The Astrophysical
Journal Letters*, *758*, L36.

De Sanctis, M. C., et al. (2013), Vesta's mineralogical composition as revealed by the
visible and infrared spectrometer on Dawn, *Meteoritics and Planetary Science*, *48*, 2166-
2184.

Ermakov, A. I. Zuber, M.T., Smith, D.E., Raymond, C.A., Balmino, G., Fu, R.R., Ivanov,
B.A., 2014. Constraints on Vesta's interior structure using gravity and shape models
from the Dawn mission. Icarus 240, 146-160.

Frigeri, A., M.C. De Sanctis, E. Ammannito, F. Tosi, F. Zambon, T.
McCord, J.P. Combe, R. Jaumann, C.A. Raymond, C.T.Russell,
The spectral parameters maps of Vesta from VIR data. Icarus, this issue.

Gaffey, M. J. (1976), Spectral reflectance characteristics of the meteorite classes, *Journal
of Geophysical Research*, *81*, 905-920.

Gaffey, M.J. (1997) Surface Lithologic Heterogeneity of Asteroid 4 Vesta, Icarus, 127,
130-157.

Konopliv, A.S., S.W. Asmar, R.S. Park, B.G. Bills, F. Centinello, A.B. Chamberlin, A.
Ermakov, R.W. Gaskell, N. Rambaux, C.A. Raymond, C.T. Russell, D.E. Smith, P.

Tricarico, M.T. Zuber, The Vesta gravity field, spin pole and rotation period, landmark positions, and ephemeris from the Dawn tracking and optical data, Icarus, Volume 240, 15 September 2014, Pages 103-117, doi.org/10.1016/j.icarus.2013.09.005.

Krohn, K., et al. (2014), Mass movement on Vesta at steep scarps and crater rims, *Icarus*, 244, 120-132. doi:10.1016/j.icarus.2014.03.013

Li, Jian-Yang, Lucy A. McFadden, Peter C. Thomas, Max J. Mutchler, Joel Wm. Parker, Eliot F. Young, Christopher T. Russell, Mark V. Sykes, Britney E. Schmidt, 2010, Photometric mapping of Asteroid (4) Vesta's southern hemisphere with Hubble Space Telescope. Icarus, 208, 238-251.

Li , Jian-Yang, J.-Ph. Combe , A. Longobardo , F. Capaccioni , M.C. De Sanctis , E. Ammannito, M.T. Capria, E. Palomba, F. Tosi, F. Zambon, S.E. Schröder, B.W. Denevi, V. Reddy, C.T. Russell, C.A. Raymond (2013). The Photometric Properties of Vesta in Visible and Near-Infrared from Dawn VIR Instrument. 44th Lunar and Planetary Science Conference, held March 18-22, 2013 in The Woodlands, Texas. LPI Contribution No. 1719, p.2343

Longobardo, A.; Palomba, E.; Capaccioni, F.; De Sanctis, M.C.; Tosi, F.; Ammannito, E.; Schröder, S.E.; Zambon, F.; Raymond, C.A.; Russell, C.T.; 2014. Photometric behavior of spectral parameters in Vesta dark and bright regions as inferred by the Dawn VIR spectrometer. Icarus 240, 20-35.

Mayne, R.G., McSween, H.Y., McCoy, T.J., Gale, A. 2009. Petrology of the unbrecciated eucrites. Geochim. Cosmochim. Acta, 73, 794-819.

McCord, T.B. , J.B. Adams, T.V. Johnson (1970). Asteroid Vesta: Spectral reflectivity and compositional implications. Science, 168 (1970), pp. 1445–1447

T.B. McCord, J.-Y. Li, J. -Ph. Combe, H.Y. McSween, R. Jaumann, V. Reddy, F. Tosi, D.A. Williams, D.T. Blewett, D. Turrini, E. Palomba, C.M. Pieters, M.C.E. De Sanctis, E. Ammannito, M.T. Capria, L. Le Corre, A. Longobardo, A. Nathues, D.W. Mittlefehldt, S.E. Schröder, H. Hiesinger, A.W. Beck, F. Capaccioni, U. Carsenty, U. Keller, B.W. Denevi, J.M. Sunshine, C.A. Raymond, C.T. Russell (2012). Dark Material on Vesta from the infall of carbonaceous volatile-rich material. Nature, 491 (2012), pp. 83–86 http://dx.doi.org/10.1038/nature11561

McFadden, L.A. et al. 2012 Mapping the mineralogical composition of the Pinaria region (Av-11) of Vesta, Geophysical Research Abstracts, Vol. 14, EGU2012-9228, 2012.

McFadden, L.A., Gaffey, M.J., Takeda, H., Jackowski, T.L., Reed, K.L. (1982) Reflectance spectroscopy of diogenite meteorite types from Antarctica and their relationship to asteroids. Symposium on Antarctic Meteorites, 7th, Tokyo, Japan,

p. 188-206.

McSween, H.Y. et al. 2013. Dawn: The Vesta-HED connection; and the geologic context for eucrites, diogenites, and howardites. DOI: 10.1111/maps.12108

McSween, H.Y et al. 2013 Composition of the Rheasilvia Basin, a window into Vesta's interior. JOURNAL OF GEOPHYSICAL RESEARCH: PLANETS, VOL. 118, 335 –346, doi:10.1002/jgre.20057, 2013

Melosh, H.J. 1989. Impact Cratering: A geologic process. Oxford University Press, New York, 253 pp.

Moriarty, D.P. and Pieters, C.M. (2015) Pryoxene Composition Derived from Absorption Band Centers, submitted to Meteoritics and Planetary Science.

Prettyman, T. H. *et al.* Elemental mapping by Dawn reveals exogenic H in Vesta's regolith. *Science* doi:10.1126/science.1225354

PRETTYMAN, Thomas H., David W. MITTLEFEHLDT, Naoyuki YAMASHITA, Andrew W. BECK, William C. FELDMAN, John S. HENDRICKS, David J. LAWRENCE, Timothy J. MCCOY, Harry Y. MCSWEEN, Patrick N. PEPLOWSKI, Robert C. REEDY,

Preusker, F., Scholten, F., Matz, K.-D., Roatsch, T., Jaumann, R., Raymond, C.A., Russell, C.T. 2014. Global Shape of (4) Vesta from Dawn FC Stereo images. Vesta in the Light of Dawn: First Exploration of a Protoplanet in the Asteroid Belt, held 3-4 February, 2014 in Houston, Texas. LPI Contribution No. 1773, p. 2027.

C. A. Raymond, R. S. Park, A. S. Konopliv, S. W. Asmar, R. Jaumann, H. Y. McSween, M. C. De Sanctis, E. Ammannito, D. L. Buczkowski, C. T. Russell, D. E. Smith, M. J. Toplis and M. T. Zuber (2014) Geophysical Constraints on the Sturcture and Evolution of Vesta's Crust and Mantle, 45th Lunar and Planetary Science Conference, 2214.

Reddy, V. Li, J-Y, LeCorre, L. Scully, J.E.C., Gaskell, R., Russell, C.T., Park, R.S., Nathues, A., Raymond, C. Gaffey, M.J., Sierks, H. Becker, K.J., McFadden, L.A. 2013, Comparing Dawn, Hubble Space Telescope, and ground-based interpretations of (4) Vesta, Icarus, 226, 1103-1114.

Roatsch, T. E. Kersten , K.-D. Matz , F. Preusker , F. Scholten , R. Jaumann , C.A. Raymond , C.T. Russell 2012 High resolution Vesta High Altitude Mapping Orbit (HAMO) Atlas derived from Dawn framing camera images Planetary and Space Science 73 (2012) 283–286

Ruesch, O., Hiesinger, H., Cloutis, E. Le Corre, L., Kallisch, J., Mann, P., Markus, K, Metzler, K., Nathues, A., Reddy, V. 2015 Near infrared spectroscopy of HED meteorites:

Effects of viewing geometry and compositional variations. Submitted to Icarus.

Russell, C.T., C.A. Raymond, A. Coradini, H.Y. McSween, M.T. Zuber, A. Nathues, M.C. De Sanctis, R. Jaumann, A.S. Konopliv, F. Preusker, S.W. Asmar, R.S. Park, R. Gaskell, H.U. Keller, S. Mottola, T. Roatch, J.E.C. Scully, D.E. Smith, P. Tricarico, M.J. Toplis, U.R. Christensen, W.C. Feldman, D.J. Lawrence, T.J. McCoy, T.H. Prettyman, R.C. Reedy, M.V. Sykes, T.N. Titus (2012). Dawn at Vesta: testing the protoplanetary paradigm. Science, pp. 684–686 http://dx.doi.org/10.1126/science.1219122

Schenk, P., D.P. O'Brien, S. Marchi, R. Gaskell, F. Preusker, T. Roatsch, R. Jaumann, D. Buczkowski, T. McCord, H.Y. McSween, D.A. Williams, A. Yingst, C. Raymond, C.T. Russell (2012). The giant Rheasilvia impact basin, the evolution of asteroid 4 Vesta and its link to meteorites. Science, 336 (2012), pp. 694–697.

Shestopalov et al. 2008 Vestoid surface composition from analysis of faint absorption bands in visible reflectance spectra, Icarus, 195, 649-662.

Shestopalov et al. 2015, LPSC abstract.

Stephan, K., et al. (2014), Small fresh impact craters on asteroid 4 Vesta: A compositional and geological fingerprint, *Journal of Geophysical Research (Planets)*, *119*, 771-797.

TOPLIS, Michael J., Lucille LE CORRE, Hugau MIZZON, Vishnu REDDY, Timothy N. TITUS, Carol A. RAYMOND, and Christopher T. RUSSELL. 2013. Neutron absorption constraints on the composition of 4 Vesta. Meteoritics & Planetary Science 48, Nr 11, 2211–2236 (2013) doi: 10.1111/maps.12244.

Tosi, F. M.T. Capria, M.C. De Sanctis, J.-Ph. Combe, F. Zambon, A. Nathues, S.E. Schröder, J.-Y. Li, E. Palomba, A. A. Longobardo, D.T. Blewett, B.W. Denevi, E. Palmer, F. Capaccioni, E. Ammannito, T.M. Titus, D.W. Mittlefehldt, J.M. Sunshine, C.T. Russell, C.A. Raymond the Dawn/VIR Team
2014. Thermal measurements of dark and bright surface features on
Vesta as derived from Dawn/VIR. Icarus 240, 36–57.

Zambon, F. et al., 2014. Spectral analysis of the bright materials on the asteroid
Vesta. Icarus 240, 73–85.